Bioorg. Med. Chem. 95 (2023) 117506

Contents lists available at ScienceDirect

Bioorganic & Medicinal Chemistry

journal homepage: www.elsevier.com/locate/bmc

Probing a distinct druggable tubulin binding site with gatorbulins 1–7, their metabolic and physicochemical properties, and pharmacological consequences

Qi-Yin Chen [a,b], Ranjala Ratnayake [a,b], Rafael Hortigüela [c], Gustavo M. Seabra [a,b], Michael D. Cameron [d], J. Fernando Díaz [c], María Ángela Oliva [c], Hendrik Luesch [a,b,*]

[a] Department of Medicinal Chemistry, University of Florida, Gainesville, FL 32610, United States
[b] Center for Natural Products, Drug Discovery and Development (CNPD3), University of Florida, Gainesville, FL 32610, United States
[c] Centro de Investigaciones Biológicas Margarita Salas, Consejo Superior de Investigaciones Científicas, Ramiro de Maeztu 9, 28040 Madrid, Spain
[d] The Herbert Wertheim UF Scripps Institute for Biomedical Innovation and Technology, 120 Scripps Way, Jupiter, FL 33458, United States

ARTICLE INFO

Keywords:
Tubulin binding
Anticancer drugs
Tubulin polymerization inhibitors
Total synthesis
Gatorbulins

ABSTRACT

Microtubules, consisting of α/β-tubulin heterodimers, are prime targets for anticancer drug discovery. Gatorbulin-1 (GB1, **1a**) is a recently described marine natural product that targets tubulin at a new, seventh pharmacological site at the tubulin intradimer interface. Using our previously developed robust route towards GB1 (**1a**), we synthesized simplified, first-generation gatorbulins, GB2–7 (**1b–1g**) of this highly modified cyclodepsipeptide (GB1) that does not contain any proteinogenic amino acid. We systematically investigated the structure-activity relationship at the biochemical and cellular level using GB1-susceptible ovarian and cervical cancer cells. We validated that the hydroxamate moiety in the *N*-methyl-alanine residue is critical for activity. All other structural modifications present in GB1, including C-hydroxylation of asparagine, methylation at C-4 of proline, and sp^2 hybridization in dehydro-alanine, were proven to be functionally relevant. Replacement of the primary amide with a methyl ester also resulted in reduced activity, indicating the intricate scaffold optimization by the GB1-producing cyanobacterium. Inhibition of tubulin polymerization *in vitro* and binding affinities correlated very well, translating into differentials in cellular efficacy. We used docking and molecular dynamics to evaluate the effects of the chemical simplification at the structural level, indicating that each modification resulted in loss of target interactions, although energetically modest. Similar to cevipabulin that targets two different sites on the tubulin dimer, GB1 promotes proteasome-mediated tubulin degradation but by an unknown mechanism, presumably distinct from that of cevipabulin. Comparison with cevipabulin indicated that this compound binds to the same tubulin region as GB1 (**1a**), although the binding mode is distinct. Cevipabulin almost exclusively interacts with α-tubulin, including nonexchangeable GTP. In contrast, GB1 (**1a**) makes extensive contact and hydrogen bonds with both α- and β-chains of tubulin. GB1-7 showed excellent solubility and much higher than that of paclitaxel. Hepatic microsome stability was excellent, human cytochrome P450s were not inhibited and plasma binding was minimal with high free fractions. Passive permeability was predicted to be high based on PAMPA. Parent compound GB1 (**1a**) was further evaluated using a cellular model with MDCK

Abbreviations: BEP, 2-bromo-1-ethyl-pyridinium tetrafluoroborate; Bn, benzyl; BOP, (benzotriazol-1-yloxy)tris-(dimethylamino)phosphonium hexafluorophosphate; BOP-Cl, bis(2-oxo-3-oxazolidinyl)phosphinic chloride; BRSM, based on recovered starting material; *t*-Bu, *tert*-butyl; CsA, cyclosporin A; DCC, *N,N'*-dicyclohexylcarbodiimide; DEPBT, 3-(diethoxyphosphoryloxy)-1,2,3-benzotriazin-4(3H)-one; DIEA, *N,N*-diisopropylethylamine; EDCI, *N*-(3-dimethylaminopropyl)-*N'*-ethylcarbodiimide hydrochloride; DMSO, Dimethylsulfoxide; FDPP, pentafluorophenyl diphenylphosphinate; Fm, Fluorenylmethyl; Fmoc, 9-fluorenylmethyloxycarbonyl; GTP, Guanosine-5′-triphosphate; HATU, bis(dimethylamino)methylene]-1H-1,2,3-triazolo[4,5-*b*]pyridinium 3-oxid hexafluorophosphate; HBTU, 2-(1H-benzotriazol-1-yl)-1,1,3,3-tetramethyluronium hexafluorophosphate; HOAt, 1-hydroxy-7-azabenzotriazole; HOBt, 1-hydroxybenzotriazole; MM/GBSA, Molecular Mechanics Generalized Born Surface Area; MTC, 2-methoxy-5-(2,3,4-trimethoxyphenyl)-2,4,6-cycloheptatrien-1-one; MTT, 3-(4,5-dimethylthiazol-2-yl)-2,5-diphenyltetrazolium bromide; PAMPA, Parallel Artificial Membrane Permeability Assay; RMSD, Root Mean Squared Deviation; SAMD, Simulated Annealing Molecular Dynamics; TBAF, tetra-*n*-butylammonium fluoride; TBS, *tert*-butyldimethylsilyl; TES, triisopropylsilyl; TIPS, t riisopropylsilyl; Trt, trityl/triphenylmethyl; TMSOTf, trimethylsilyl trifluoromethanesulfonate; PyAOP, (7-azabenzotriazol-1-yloxy)- tripyrrolidinophosphonium hexafluorophosphate; PyBOP, (benzotriazol-1-yloxy)tripyrrolidinophosphonium hexafluorophosphate; PyBrOP, bromotripyrrolidinophosphonium hexafluorophosphate.

* Corresponding author at: Department of Medicinal Chemistry, University of Florida, Gainesville, FL 32610, United States.
E-mail address: luesch@cop.ufl.edu (H. Luesch).

https://doi.org/10.1016/j.bmc.2023.117506
Received 16 September 2023; Received in revised form 19 October 2023; Accepted 20 October 2023
Available online 21 October 2023

cells stably transduced with the human efflux transporter MDR1/P-gp, showing similar permeability with and against transporter gradient, indicating that GB1 (**1a**) is a poor P-gp substrate.

1. Introduction

Microtubules consist of α/β-tubulin heterodimers that are assembled into longitudinal protofilaments, held together through lateral interactions[1]. They are critical and highly dynamic components of the cytoskeleton of eukaryotic cells, form mitotic spindles, and serve for intracellular trafficking[2],but also regulate inflammatory and oncogenic signaling[3,4]. Modulation of tubulin dynamics, either stabilizing or destabilizing microtubules, has been highly rewarding for drug discovery. Specifically, tubulin is a validated target for anticancer therapeutic discovery[5]. Seven druggable sites targeted by natural products have been identified, three of which already led to FDA-approved cancer drugs, including the maytansine site, vinca site, and the taxane site[5,6]. The natural product ligand targeting the colchicine site is approved for the prevention and treatment of attacks of gout. There is a demand for tubulin agents that exert their function through distinct binding to tubulin at α- or β-tubulin or interfaces.

Marine cyanobacteria have previously yielded tubulin-targeting dolastatin 10, which provided the starting point for five FDA-approved antibody-drug conjugates[7]. We recently identified the seventh pharmacological site targeted by gatorbulin-1 (GB1, **1a**, Fig. 1), a marine natural product from a Floridian cyanobacterium that destabilizes microtubule, presumably through a new mechanism[6]. GB1 possesses pharmacological and structural novelty, distinguished by being a highly modified depsipeptide (Fig. 1A) without any standard proteinogenic amino acid. We validated the structure by total synthesis, probed the mechanism of action, performed biochemical experiments to determine the inhibitory effects on tubulin polymerization and indirect effects on the adjacent colchicine site, and visualized the α/β-tubulin-GB1 complex at high resolution by X-ray analysis (Fig. 1B and 1C), demonstrating the novelty on multiple levels[6]. We also assessed the cellular activity against breast, cervical and ovarian cancer cell lines, which are generally susceptible to microtubule targeting agents[8].

We had also previously isolated the *N*-deoxy analogue of GB1, which lacked activity against cancer cells[6], suggesting that the *N*-hydroxylation of alanine is critical for binding or cellular stability.

To determine if all of the amino modifications are crucial for activity and with the goal to identify tunable elements and obtaining an understanding of the structure–activity relationship (SAR), here we probed the gatorbulin site with simplified gatorbulins, which we synthesized and tested alongside GB1 for effects on tubulin polymerization, binding affinity and cancer cell viability, and interrogated the binding site using molecular docking approaches. We also compared the binding site of gatorbulins with that of cevipabulin (Fig. 2), a synthetic dual-targeting tubulin agent at the vinblastine site and at also another site in the region of the gatorbulin site[9]; however, predominantly interacting with α-tubulin near the non-exchangeable GTP. We assessed the metabolic and physicochemical properties of gatorbulins and also compared the pharmacological consequences with respect to tubulin stability in ovarian cancer cells.

2. Results and discussion

2.1. Chemistry

Through chemical synthesis and medicinal chemistry, we aimed at systematically simplifying the gatorbulin structure to probe the importance of the modifying elements that confer structural uniqueness to GB1 with respect to the biochemical and cellular activity and mechanism. Our first-generation analogues focused on the modulation of current groups as highlighted in Fig. 3: *N*-deoxy analogue of hydroxamic acid (GB2, **1b**, natural product)[6], Asn analogue (GB3, **1c**), methyl ester instead of primary amide (GB4, **1d**), Pro analogue (GB5, **1e**), replacement of dehydro-Ala (dhAla) with *S*-Ala (GB6, **1f**) and *R*-Ala (GB7, **1g**).

Retrosynthetic Analysis. Fig. 4 depicts the general retrosynthetic analysis of the simplified analogues. Similar to the synthetic strategy of GB1 (**1a**) (Figure S1), the proposed analogues **1b-1g** (Fig. 3) resulted from the global unmasking of cyclized precursors **2b-2 g**. The site between of (Me)Pro and (SePh)Ala was chosen for macrolactamization. Fmoc-Fm pair was chosen as the protection groups of amino and carboxy termini, respectively, because they could be cleaved simultaneously by

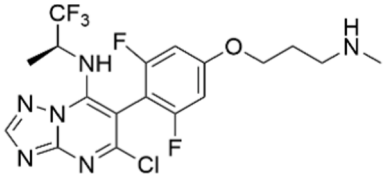

Fig. 2. Chemical structure of cevipabulin.

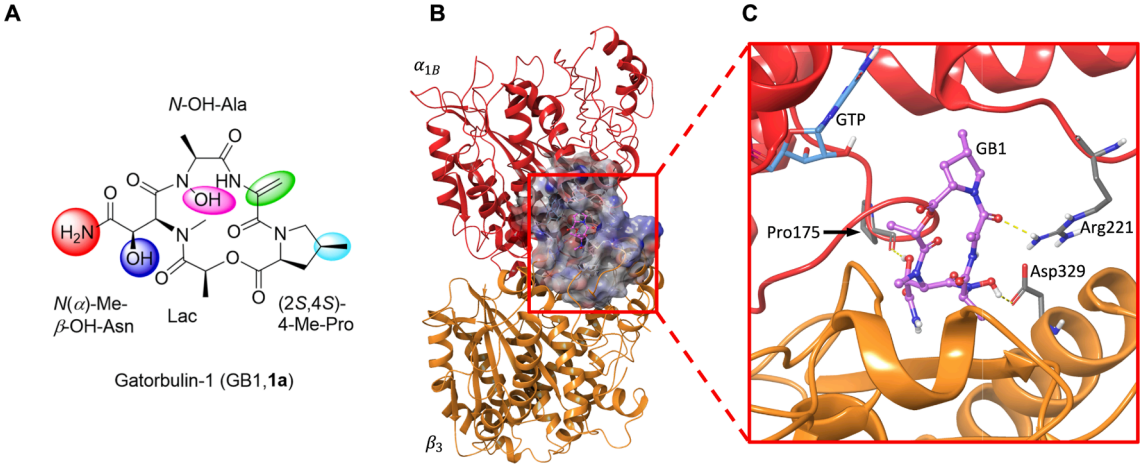

Fig. 1. Gatorbulin-1 (GB1, **1a**) structure and target interaction. (A) Chemical structure. (B, C) Crystal structure of α/β-tubulin in complex with GB1 from PDBID 7ALR.[6] GTP is visible in blue sticks in the upper left region of (C).

the mediation of secondary amines[10]. The linear compounds **3b-3 g** were disconnected into four units: Asp/Asn **4**, Ala derivatives **5**, proline ester acid **6** and Ala derivative **7**; and proline ester acid **6** were further disassembled into two commercially available subunits lactate **8** and proline derivative **9**. We chose allyl rather than benzyl as *N*-OH protecting group since allyl could be removed selectively by $Pd(Ph_3P)_4$ in the presence of dehydro-peptide; however, when benzyl was used, the hydrogenation at the debenzylation stage reduced dehydro-Ala simultaneously, irrespective of hydrogen gas or transfer hydrogen donor (e.g. 1,4-cyclohexadiene, ammonium formate, etc.) was used in the reaction. Choosing *tert*-butyl for the carboxyl protection of **5a** enabled selective removal by TMSOTf/2,6-lutidine in presence of allyl, TBS and Fmoc groups[6,11,12]. Most of the building blocks were synthesized in our previous work or are commercially available.

We established a practical and robust synthetic route for GB1 (**1a**)[6]. The synthetic routes to the new analogues paralleled that for GB1 (**1a**, Scheme S1) and the compounds are numbered based on those compounds in the synthesis of GB1 (**1a**, Supporting Information Figure S1 and Scheme S1).

Synthesis of GB2 (**1b**). GB2 (**1b**) was co-isolated with GB1 from marine cyanobacteria as a minor constituent, insufficient for rigorous biological testing[6]. The hydroxamic acid group (NOH) of GB1 (**1a**) plays a critical role in binding with tubulin based on cocrystal structure analysis[6]. To verify its role as well as for SAR elucidation, we carried out the total synthesis of GB2 (**1b**) (Scheme 1). We followed the general synthetic strategy (Fig. 4) and the synthesis of GB1 (**1a**) (Figure S1, Scheme S1) to synthesize GB2 (**1b**). The synthetic protocols of building blocks **4a, 6a** and **7a** were reported in our previous work[6]. The standard coupling of **4a** with benzyl ester-Ala (**5b**) mediated by HBTU/HOBt provided **10b** in moderate yield. We chose benzyl rather than *tert*-butyl as the carboxy protection group of **10b** because in the next deprotection step, compound **12b** and its *tert*-butyl ester (parallel to **12a** and **11a**, respectively) were not stable under deprotection condition (TMSOTf/2,6-lutidine) to remove the *tert*-butyl group (Scheme 1, from **11b** to **12b**). The Fmoc group of compound **10b** was cleaved by Et_2NH in MeCN and the released corresponding amine then coupled with **6a** using 2-bromo-1-ethyl-pyridinium tetrafluoroborate–mediated coupling (BEP)[13] to produce **11b** in 93 % yield for two steps. In the total synthesis of **1a** (Scheme S1)[6], we had screened various coupling reagents for the methylamino coupling of **10a** with **6a** (Table 1), and finally BEP emerged as the best coupling reagent, which we applied it for the synthesis of all other analogues. Hydrogenation of **11b** with $Pd/C/H_2$ in MeOH gave acid **12b** in 90 % yield. However, as mentioned above, when *tert*-butyl was used to mask the carboxyl group of **11b**, the yield of acid **12b** was as low as 15 % since **12b** or its *tert*-butyl ester was unstable upon exposure to TMSOTf /2,6-lutidine. The coupling of acid **12b** with the amine derived from **7a** by BOP in THF provided linear compound **3b** in excellent yield, 92 %.

Amino protecting group Fmoc and carboxy protecting group Fm were removed simultaneously by Et_2NH in MeCN and the resulting free amino acid was subjected to macrocyclization under the mediation by PyBOP/HOAt to yield cyclized compounds **2b** in a reasonable yield 27 % over two steps. Along with saturated selenium product **2b**, a minor, dehydrated product was isolated (**dh-2b**, 3–4 % yield). For the macrocyclization, we had screened series of coupling reagents when we prepared **2a** (Table 2, Scheme S1) and found PyBOP/HOAt could provide optimal condition with good yield of **2a** (~61 %) but low yield of dehydrated product **dh-2a** (~3 %). Therefore, we applied the combination of PyBOP/HOAt in all macrocyclization reactions. Fully deprotection of **2b** to yield **1b** is depicted in Scheme 1. The cleavage of TBS group of **2b** was mediated by TBAF/HOAc (10 eq.:12 eq.) buffer to provide free alcohol **13b** in 80 % yield. Subsequent oxidative elimination of SePh group of **13b** with $NaIO_4$ (4 eq.) yielded corresponding dehydro-peptide **14b**. The exposure of **14b** to the solution of TFA in CH_2Cl_2 (1:5, v/v) without scavenger led to the cleavage of trityl group and yielded final product GB2 (**1b**) in 38 % yield. We found that using hydrosilane (TIPS or TES) as scavenger in the deprotection of **14a** (Scheme S1) resulted in a very low yield; presumably part of reactant **14a** degraded as its dehydro-Ala moiety is sensitive to the reduction property of TIPS/TES in TFA[14,15]. Final product **1b** was purified by reversed-phase TLC plate (C18). The synthetic GB2 (**1b**) was identical to the isolated natural product, which was verified by NMR, HRMS and optical rotation.

Synthesis of GB3 (1c). To probe the role of the β-hydroxy group in the asparagine-derived unit of GB1(**1a**), we designed GB3 (**1c**, Fig. 3) in which β-hydroxy Asn was replaced by Asn. The total synthesis strategy for GB3 (**1c**) is depicted in Scheme 2. Acid *N*-Me-*N*-Fmoc-Asp(OMe) (**4b**) was activated to the acid chloride by $(COCl)_2$ and then subjected to amidation by **5a** in the presence of AgCN to afford product **16** in 78 % yield[6,16,17]. The methyl ester group of **16** was hydrolyzed with Me_3SnOH in 1,2-dichloroethane (DCE) under reflux to give acid **17**[18]. Coupling of **17** with triphenylmethylamine ($TrtNH_2$) gave **10c** in 73 % yield (40 % yield for total 4 steps). The coupling of $TrtNH_2$ was a challenging to accomplish, presumably due to considerable steric hindrance. We succeeded using the acid chloride method and screened various coupling reagents including EDCI, HBTU, BEP, PyBrOP and PyAOP; PyAOP gave the best yield (73 %) while others gave low to modest yields (trace to 30 % yield) or caused difficulty for purification. It is noteworthy that we did

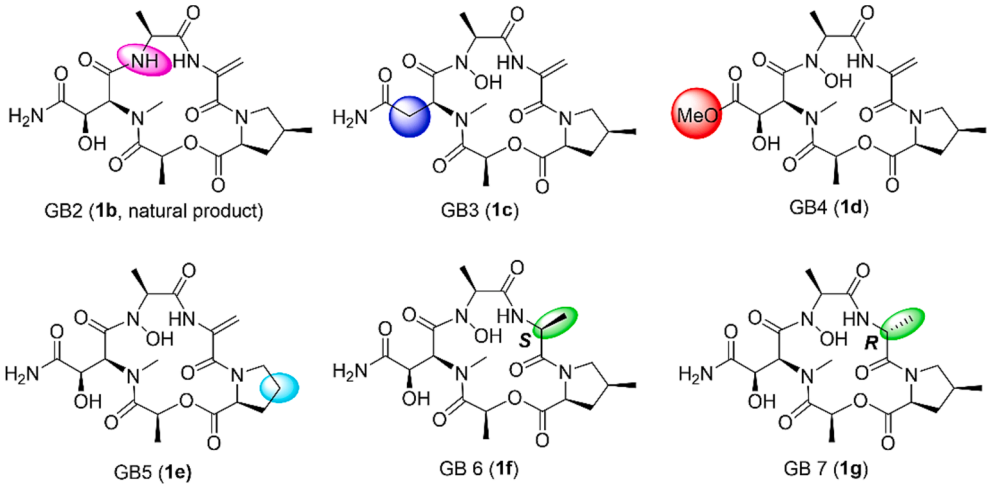

Fig. 3. Chemical structures of gatorbulin-2 (GB2, **1b**) and newly designed simplified analogues GB3-7 (**1c-1g**). Modified positions are highlighted and colors correlate with Fig. 1A.

not use commercially available *N*-Me-*N*-Fmoc-Asn(Trt) (**4d**) immediately to prepare **10c**, because the amidation of **4d** with **5a** using the same method failed; no amidation product was detected. NMR and MS analysis suggested that that the trityl group was cleaved. This speculation was confirmed by the success of reaction of **4b** (*N*-Me-*N*-Fmoc-Asp (OMe)) with **5a**. Possibly the absence of OTBS (lack of steric hindrance) facilitated the accessibility of the tritylamide by electrophiles.

The Fmoc group of compounds **10c** were cleaved by Et_2NH in MeCN and the released corresponding free amine was coupled with **6a** using BEP to afford product **11c** in 90 % yield over two steps. The *tert*-butyl group of **11c** was removed using a mixture of TMSOTf /2,6-lutidine to provide corresponding acid **12c** in excellent yield (93 %). BOP-mediated coupling of acid **12c** with the free amine derived from **7a** in THF provided linear compound **3c** in 80 % yield. Amino protecting group Fmoc and carboxy protecting group Fm were removed simultaneously by Et_2NH in MeCN and the resulting free amino acid was subjected to macrocyclization under the mediation of PyBOP/HOAt to yield cyclized compound **2c** in 39 % yield over two steps.

Along with saturated selenium products **2c**, we also detected a minor dehydrated product (**dh-2c**, 3–4 % yield). Total deprotection of **2c** using standard conditions to provide **1c** is depicted in Scheme 2. Oxidative elimination of SePh group of **2c** with $NaIO_4$ (4 eq.) yielded corresponding dehydro-peptide **14c**[6,19]. Exposure of **14c** to the solution of TFA in CH_2Cl_2 (1:5, v/v) without scavengers cleaved the trityl group and yielded primary amide **15c**. Removal of the allyl group of **15c** by Pd $(PPh_3)_4/PhSiH_3$[6,20] provided final product GB3 (**1c**) in 64 % yield upon purification by reversed-phase TLC plate (C18).

Syntheses of GB4–7 (**1d–1g**). Based on the general retrosynthetic analysis for GB4 (**1d**), we first needed to synthesize **4c**, as shown in Scheme 3. The *N*-Me-β-OH-Asp(OMe)–OH (**18**) was synthesized from (*2R*,*3R*)-epoxysuccinic acid by aminolysis and successive esterification[6]. The methylamino group, carboxyl group and β-OH of **18** were protected in order by Fmoc, benzyl and TBS using standard procedures to give intermediates **19**, **20** and **21**, respectively (Scheme 3). Masking of the carboxyl group of **19** as Bn esters (**20**, **21**) simplified the separation and purification compared with the corresponding carboxylic acids. Hydrogenation of **21** with Pd/C/H_2 in MeOH provided carboxylic acid **4c** in good yield (89 %). The necessity to protect the β-OH of **4a**, **b** (by TBS) is noteworthy as free OH would cause side reactions when **4** was activated to acid chloride and coupled with **5a**, and it could compete for acylation with methylamino at the installation stage of building block of **6a**. Acid **4a** was synthesized following the same protocol we previously published[6].

Scheme 4 outlines the optimized synthetic route and strategy for the synthesis of linear precursors **3d-g**, cyclized precursors **2d-g** and final targets **1d-g**. Compound **5a**, **6a** and **7a** were synthesized following the original protocol for GB1[6] and **6b** was synthesized by another published protocol[21]; compound **5b**,**7b**, 7**c** are commercially available (Fig. 4). With the building blocks in hand, they were sequentially fused into linear precursors **3d-3 g**, cyclized precursor **2d-2 g** and final products **1d-1g**.

Using the similar procedure as published[16,17] with minor modification, full masked acids **4c** and **4a** were converted to acid chlorides using oxalyl chloride in toluene and then coupled with **5a** using AgCN as base in toluene at 80 °C to provide compounds **10d** and **10a**, respectively, in 60–70 % yield. We replaced benzene with toluene for toxicity reasons, without sacrificing yield.

The Fmoc group of compounds **10d** and **10a** was cleaved by Et_2NH in MeCN and the resulting corresponding free amines then coupled with **6a** and **6b**, respectively, using BEP as coupling reagent to produce products **11d** (from **10d**, **6a**), **11e** (from **10a**, **6b**), and **11a** (from **10a**, **6a)** in good yields (78–90 %). The *tert*-butyl groups of **11d**, **11e**, and **11a** were removed by the buffer of TMSOTf /2,6-lutidine to provide corresponding acids **12d**, **12e**, and **12a**. Coupling of acids **12d**, **12e**, and **12a** with the amines derived from **7a**, 7**b**, and **7c** by BOP in THF provided linear compounds **3d** (from **12d**, **7a**), **3e** (from **12e, 7a**), **3f** (from **12a**, **7b**) and **3 g** (from **12a**, **7c**) in excellent yields 80–96 %.

Amino protecting group Fmoc and carboxy protecting group Fm of **3d-3 g** were removed simultaneously by Et_2NH in MeCN and the resulting free amino acids were subjected to macrocyclization under the mediation of PyBOP/HOAt to yield the corresponding cyclized compounds **2d-2 g** in reasonable yields (32–57 %). Along with saturated selenium products **2d-2 g**, minor dehydrated products were isolated (**dh-2d–dh-2 g,** 3–4 % yields). Standard full deprotection of **2d-2 g** to

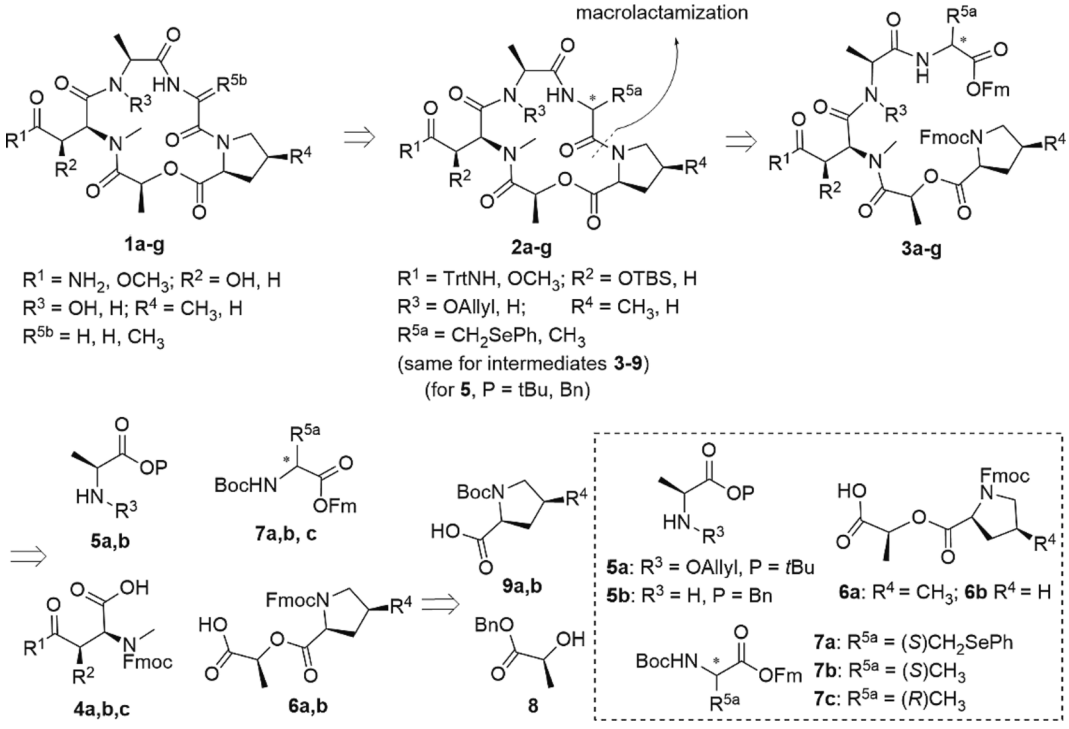

Fig. 4. General retrosynthetic analysis of GB2-7 (**1b-1g**).

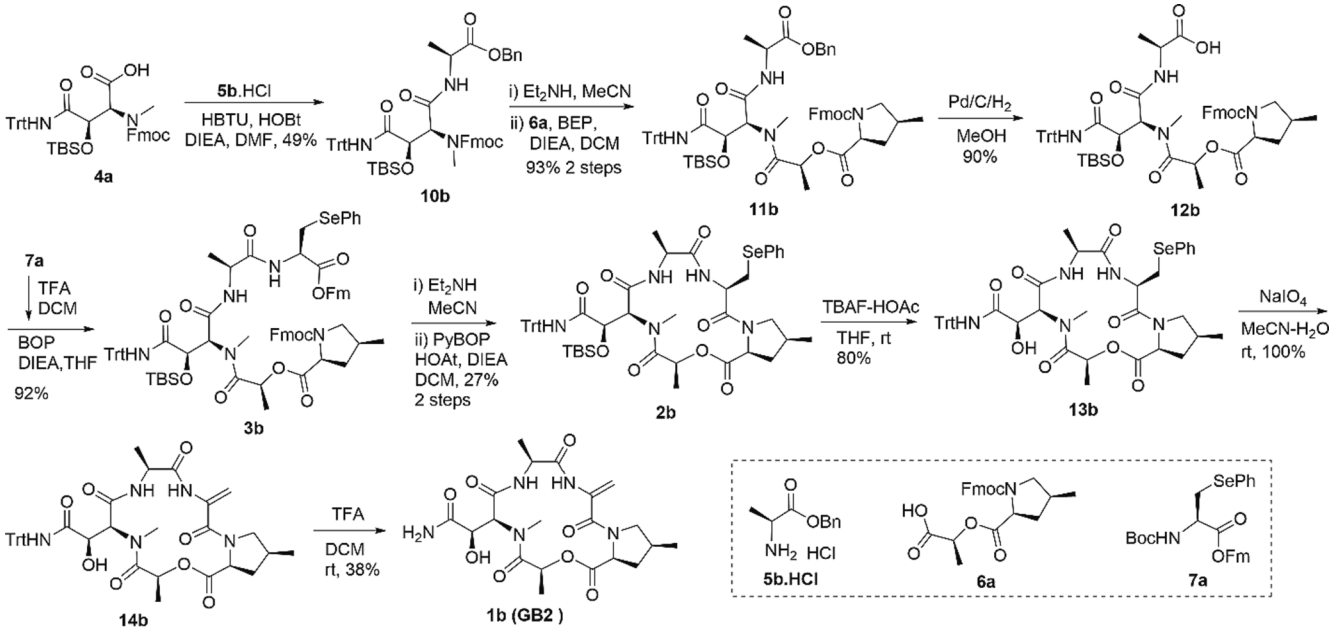

Scheme 1. The synthesis of GB2 (**1b**).

Table 1
Coupling reagents screening for the coupling reaction of **10a** with **6a.**[a]

Coupling reagent	HATU	BOP-Cl	BOP	DEPBT	DCC	BTC	PyBrOP	FDPP	BEP
Yield (%)	22	28	trace	trace	0	54	50[b]	trace	79

[a] See Scheme S1.
[b] Complex mixture.

Table 2
Coupling reagents screening for the preparation of **2a** by macrocyclization from **3a.**[a]

Coupling reagent	HATU HOAt	PyBOP HOAt	BOP	EDCI HOAt
Yield of **2a** (%)	39[b]	61.5[b]	30	47
Yield of **dh-2a** (%)	13[b]	3.2[b]	19	17

[a] See Scheme S1.
[b] Average value from multiple experiments.

afford **1d-1g** is depicted in Scheme 4. The cleavage of TBS groups of **2d-2 g** was mediated by buffer of TBAF/HOAc (10 eq.:12 eq.) to provide the corresponding free.

alcohols **13d-13 g**. Subsequent oxidative elimination of SePh group of **13d** and **13e** with $NaIO_4$ (4 eq.) yielded the corresponding dehydropeptides **14d** and **14e**. Exposure of **14e**, **13f**, and **13 g** to the solution of TFA in CH_2Cl_2 (1:5, v/v) without scavenger cleaved the trityl groups and yielded the corresponding primary.

amides **15e–15 g**, respectively. The removal of allyl group of **14d** and **15e–15 g** by $Pd(PPh_3)_4/PhSiH_3$ provided the corresponding final products GB4–7 (**1d-1g**), respectively. The yields for the final step varied from 46 to 74 %. All final products were purified by reversed-phase TLC plate (C18).

Notably, the NMR spectra of gatorbulins in DMF-d_7 (similarly in DMSO-d_6) showed the presence of two conformers. The ratio of each analogue based on ^{1}H NMR is listed in Table 3. For GB1 (**1a**), GB2 (**1b**) and GB7 (**1g**), the conformers were detected in roughly equal distribution; for GB3 (**1c**), GB4 (**1d**) and GB5 (**1e**), one conformer was dominant ranging at 60–83 %, while for GB6 (**1f**) there was only one conformer observed on the NMR timescale, which may or may not have biological implications. The spectra of all synthetic intermediates and gatorbulins are available in the Supporting Information (Figures S2–S96).

2.2. Biology

We previously demonstrated that GB1 (**1a**) directly inhibits tubulin polymerization *in vitro*[6]. GB1 (**1a**) affected tubulin assembly similar to podophyllotoxin, a colchicine site agent that also destabilize tubulin assembly and we used as control (Fig. 5A). From the other six GB derivates, only GB5 (**1e**) and GB6 (**1g**) showed a potent inhibitory effect, whereas GB4 (**1d**) had a very mild effect (Fig. 5A). These results correlated very well with binding affinities measured using a fluorescent probe for the colchicine site 2-methoxy-5-(2,3,4-trimethoxyphenyl)-2,4,6-cycloheptatrien-1-one (MTC) that preclude gatorbulin binding (Fig. 5B). We have shown previously that the β-tubulin loop T7 and α-tubulin loop T5 imperatively change conformations upon colchicine binding to avoid steric clashes and that the presence of GB1 precludes simultaneous binding of ligands at both colchicine and gatorbulin sites[6]. As control, in these experiments GB1 (**1a**) showed an affinity of $2.2 \pm 0.7 \times 10^6$ M^{-1}, which is close to the 1.01×10^6 M^{-1} we reported previously[6]. GB2 (**1b**), GB3 (**1c**) and GB7 (**1g**) showed no MTC displacement while GB4-6 (**1d-1f**) have an affinity in the 10^4 M^{-1} range (Table 4). This can be rationalized by the crystal structure previously obtained of the α/β-tubulin-GB1 complex (PDB 7ALR)[6]. The lack of *N*-hydroxylation (GB2, **1b**) or C-hydroxylation (GB3, **1c**) induced the loss of two (one with αR221 and one with βD329) and three (with α-tubulin T5 loop, αP175 and αS178) hydrogen bonds, respectively. These must be essential for the correct binding of the molecule as denoted by the lack of probe displacement and hence, binding to tubulin. The conversion of the primary amide to the methyl ester (GB4, **1d**) also affects to the formation of two hydrogen bonds with βV353 (in one of them the compound is the donor). These interactions might not be critical for the initial recognition of the compound by tubulin but should increase the affinity.

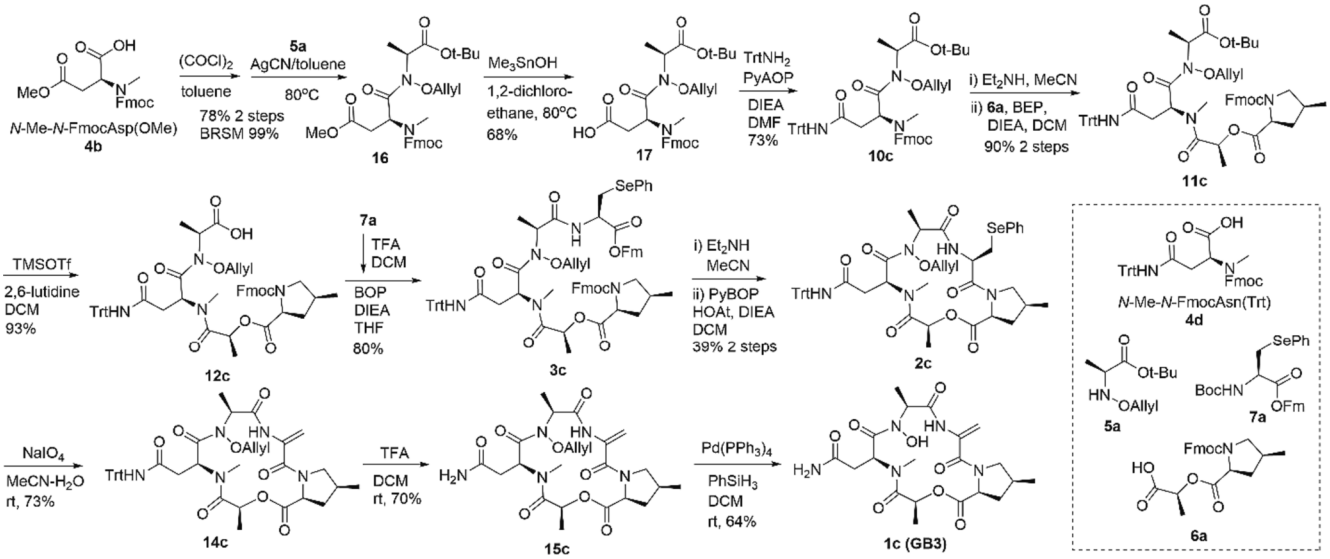

Scheme 2. Synthesis of GB3 (**1c**).

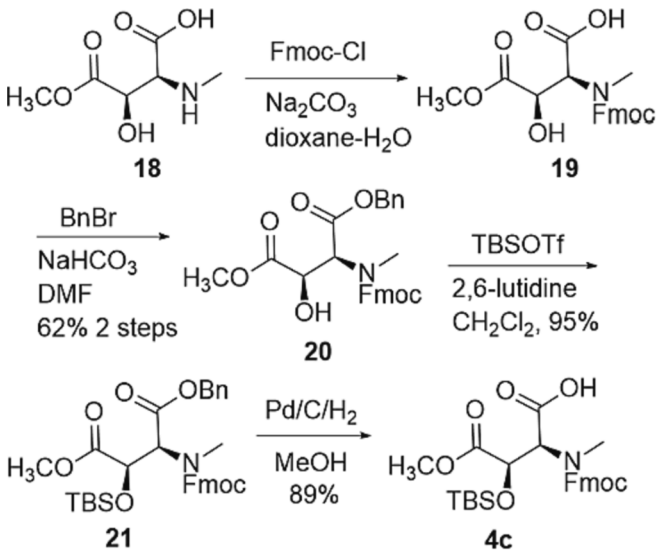

Scheme 3. Synthesis of fragment **4c**.

Removing the methyl group at the proline ring (GB5, **1e**) will affect to the formation of a couple of hydrophobic interactions with α-tubulin. Again, these interactions are not essential for initial recognition but might contribute to gaining affinity. Finally, the change in hybridization by substitution of dehydroalanine with L- or D-alanine (GB6/GB7, **1f**/**1g**) also affect the interaction. In principle the sp^2 CH_2 in GB1 (**1a**) is not involved in any contact but only the S form appears to bind to tubulin, which suggest a specific molecule conformation prone to the interaction with tubulin.

A subsequent cell-based study using SK-OV-3 ovarian and HeLa cervical cancer cells that were highly susceptible to GB1 (Fig. 5C and 5D)[6] confirmed the activity pattern observed in the biochemical assays. While GB1 (**1a**) was active at submicromolar concentrations, GB2 (**1b**), GB3 (**1c**) and GB7 (**1f**) did not show any antiproliferative activity or cytotoxicity (IC_{50} greater than 100 μM). GB4 (**1d**) and GB5 (**1e**) retained some level of activity but lost potency by 11- to 67-fold (GB4, **1d**) and 25- to 68-fold (GB5, **1e**) against SK-OV-3 and HeLa cells, respectively. GB6 (**1f**) was only active at 50–100 μM (Table 4; Fig. 5C and 5D).

In recent study it has been shown that cevipabulin also binds to the gatorbulin binding site (in addition to the vinblastine site), although in a different manner, and induces tubulin heterodimer degradation[9,22]. In order to investigate whether GB1 (**1a**) has a similar effect on tubulin degradation we carried out immunoblotting study in SK-OV-3 ovarian cancer cells in the presence or absence of the proteasome inhibitor MG132 (Fig. 5E and 5F). Similar to cevipabulin it was observed that GB1 (**1a**) also induced a reduction of both α- and β-tubulin levels in SK-OV-3 cells in a dose dependent manner. The proteasome inhibition by MG132 was able to prevent the tubulin degradation effect caused by GB1, indicating that the induced tubulin degradation is mediated by the proteasome.

Cevipabulin is known to bind simultaneously to the vinblastine and the gatorbulin sites[9], while tubulin cevipabulin-induced degradation is known to occur through binding to the new site, which is located near the non-exchangeable GTP site on the α-tubulin subunit[9]. Based on immunoblotting analysis, we found that GB1 (**1a**) also promotes proteasomal degradation of α- and β-tubulin. GB1 treatment for 16 h reduced levels of both proteins in a concentration-dependent manner (Fig. 5E and 5F). While α-tubulin levels were reduced by 80 % only at 10 μM, without substantial effect at lower concentrations, β-tubulin was depleted by 80 % at 3.2 μM, suggesting a ~ 3-fold preference for β-tubulin. Pre-incubation with the proteasome inhibitor MG132 attenuated or prevented degradation, indicating that the tubulin depletion is proteasome mediated (Fig. 5E and 5F). The mechanism is expected to be distinct to that of cevipabulin because GB1 does not contact with non-exchangeable a-tubulin GTP. Instead, cevipabulin makes the non-exchangeable GTP exchangeable and, lossing of GTP leads to tubulin destabilization and consequently unfolding and degradation[9]. Notice that cevipabulin and GB1 are biochemically distinct because cevipabulin exerts dual targeting (vinca and gatorbulin sites) and promotes *in vitro* tubulin polymerization (as vinblastine does)[23], while this mixed pharmacology is not known for gatorbulins. The mechanism of tubulin degradation by GB1 remains to be determined.

2.3. Computational modeling

Docking. Table 5 shows the results for the best poses obtained from the dockings, and the docking modes are shown in Fig. 6. The RMSD is calculated using only the non-hydrogen atoms that are present in all gatorbulins. Glide was unable to generate a docked conformation for GB7 (**1g**), indicating that the methyl group in the *R* configuration forces a large distortion, such that the compound no longer fits in the pocket. All other gatorbulins fit well into the intradimer binding pocket, with poses very similar to GB1 (**1a**) binding pose from the crystal structure.

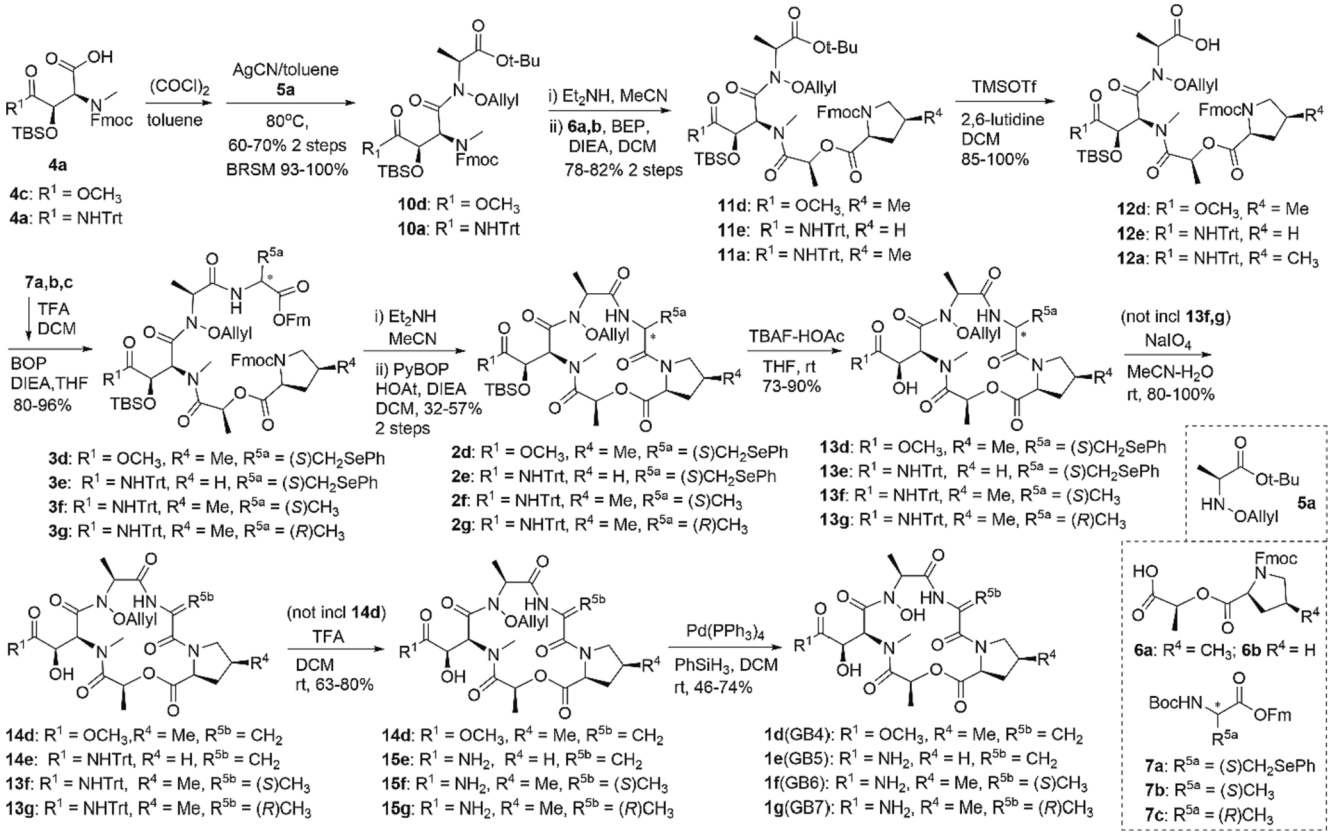

Scheme 4. Synthesis of GB4-7 (**1d-1g**).

Table 3
^{1}H NMR conformational ratios for GB1–7 (**1a**–**1g**) in DMF-d_7.

Compound	GB1 (**1a**)	GB2 (**1b**)	GB3 (**1c**)	GB4 (**1d**)	GB5 (**1e**)	GB6 (**1f**)	GB7 (**1g**)
Conformer 1/ 2 ratio	1/1	5.5/ 4.5	2/1	3/2	5/1	1/0	5.3/ 4.7

GB1 (**1a**) is in favorable position to establish H-bonds with Ser178 (2H-bonds), Gln176, Pro175, and Arg221 from α-tubulin, and Asp329 and Val353 from β-tubulin. Most of those are conserved in GB2–GB6 (**1b**–**1f**) ligands. However, in GB2 (**1b**) the hydrogen bond to βAsp329 seems weaker, and in GB3 (**1c**) the removal of the OH group leads to loss of the double hydrogen bond to αSer178. The removal of the NH_2 group in GB4 (**1d**) leads to loss of the hydrogen bond to the αPro175 backbone. Removal of the methyl group in GB5 (**1e**) leads to loss of important interactions with the hydrophobic pocket. Finally, the methyl group in GB6 (**1f**) allows nonpolar interactions with βMet325 and improves fitting in to the pocket. Those changes are reflected in the MM-GBSA energies, which indicate GB1 (**1a**), GB4 (**1d**), GB5 (**1e**) and GB6 (**1f**) as the stronger binders, and GB2 (**1b**) and GB3 (**1c**) as the weakest (Table 5), which is consistent with the multidimensional SAR data. However, the binding energies are all within too narrow a range to clearly differentiate the molecules within each group. Still, it is clear that, in all analogues, important interactions are lost compared with GB1 (**1a**).

Simulated annealing molecular dynamics. SAMD calculations were done to probe the solution structure of the compounds. Following the experimental NMR data, which indicates at most two conformers in solution, the structures were split into two clusters. In all cases one cluster dominated with over 88 % of the structures and the cluster representative structure is essentially identical to the bound conformation of GB1 crystal structure, as indicated by the RMSD measurements in Table 6. The only exceptions are GB6 and GB7, where the absence of the double bond on the DhAla residue allows for more distortion on the ring structure.

Fig. 7 shows the GB1 representative structures obtained for each cluster SAMD calculations (other molecules are in Figure S97). A common difference between the conformations in the two clusters is a 180° inversion around the H_N–N–C_α–C_β dihedral angle in the DhAla residue, again except for GB6 (**1f**) and GB7 (**1g**), which allows extra ring flexibility. In the case of GB6 (**1f**), the methyl in the *S* configuration points towards the solvent, and the distortion with respect to GB1 is due to the angle change from sp^2 to sp^3 hybridization states in the DhAla-C_α. In GB7 (**1g**), the *R* configuration would position the methyl group pointing to the ring interior, leading to steric clashes with the ester oxygen in lactic acid and the proline atoms across the ring. The clashes are avoided by a large distortion inverting the orientation around the peptide bond between residues 1 and 2, resulting in a larger ring that cannot fit inside the binding pocket.

Comparison of GB1 and cevipabulin binding to tubulin site. Cevipabulin, targeting the vinca site, has additionally been determined to also bind to the same tubulin region as GB1 (**1a**), although the binding mode is distinct. Fig. 8 compares the structures for the tubulin complexes with cevipabulin (PDB 7DP8)[9] and GB1 (**1a**) (PDB 7ALR)[6]. Both ligands present a similar total (unbound) solvent accessible surface area (676 Å^2 for cevipabulin, 629 Å^2 for GB1, Figure S98).

However, π-π in the case of cevipabulin, only about 70 % of this area is in contact with the protein, and almost exclusively with the α2 chain (68 %), where the triazolopyrimidinyl moiety is engaged in stacking with α Tyr224 and GTP. In contrast, GB1 (**1a**) makes extensive contact with both α (53 %) and β (47 %) chains and makes H-bonds to αArg221 and αPro175, and βAsp329 (Figure S99).

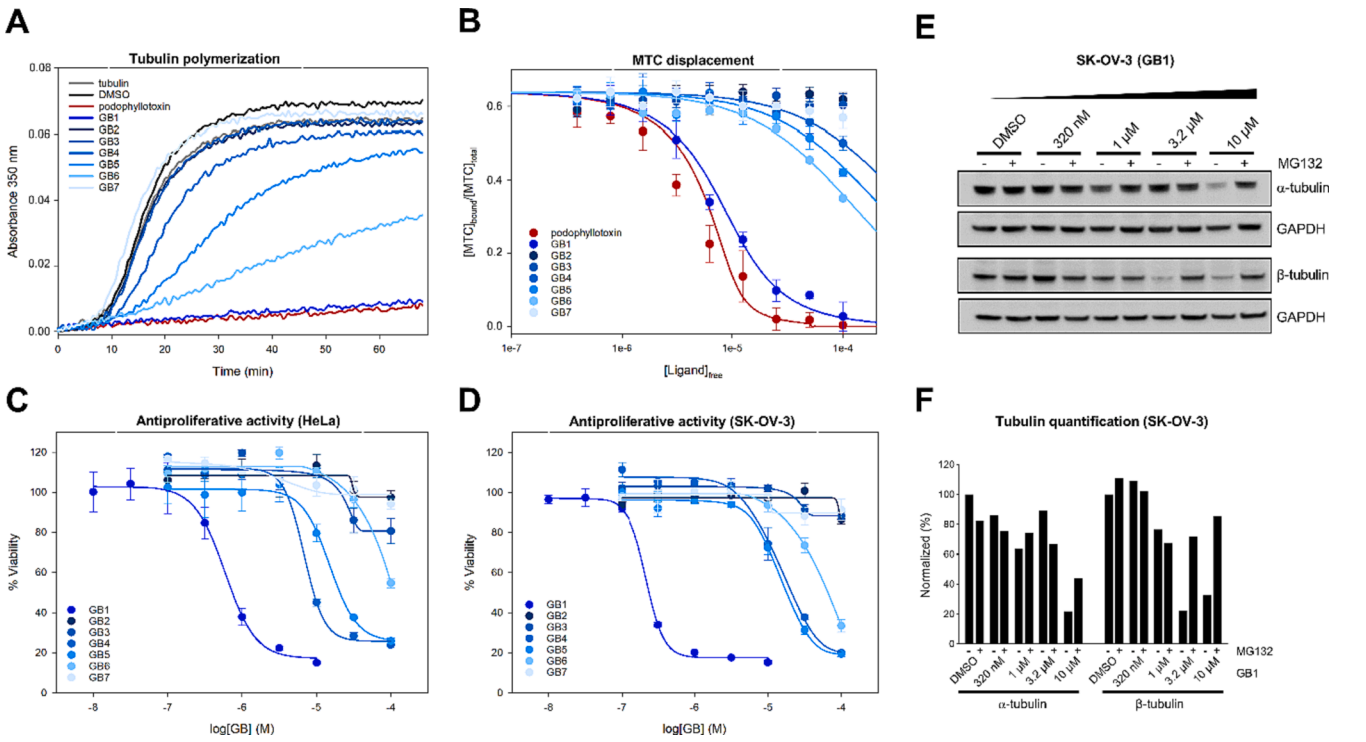

Fig. 5. Effect of gatorbulins on tubulin assembly and ovarian cancer cells proliferation. A) Time course polymerization of 25 μM tubulin in GAB buffer, in the absence (gray line) or the presence of vehicle (DMSO, black line) or 27.5 μM of gatorbulins studied (blue gradient colors lines) or tubulin inhibitor control drug podophyllotoxin (red line); B) Binding affinity of gartorbulins studied (blue gradient colors lines) compared to podophyllotoxin (red line, 1.5×10^7 M^{-1}), measured from MTC displacement assays; C-D) Percent cell viability normalized to vehicle control (0.5 % DMSO) measured by MTT assay of HeLa cervical cells (C) and, SK-OV-3 ovarian cells (D) treated with increasing concentrations of gatorbulins for 48 h; E) Western blot analysis of α- and β-tubulin levels in SK-OV-3 ovarian cells after treatment with GB1 (**1a**) at different concentrations for 16 h with (+) or without (-) pre-incubation with proteasome inhibitor (MG132, 10 μM final concentration). F) Tubulin quantification using densitometry with samples normalized to GAPDH loading control and further normalized to DMSO without MG132.

Table 4
Binding affinities (MTC) and IC_{50} values for gatorbulins in ovarian and cervical cancer cell lines.

Compound		Cell line (IC_{50})	
	K_b	SK-OV-3	HeLa
GB1 (**1a**)	$2.2 \pm 0.7 \times 10^6$ M^{-1}	216 nM	590 nM
GB2 (**1b**)	$< 1 \times 10^4$ M^{-1}	>100 μM	>100 μM
GB3 (**1c**)	$< 1 \times 10^4$ M^{-1}	>100 μM	>100 μM
GB4 (**1d**)	$1.5 \pm 0.5 \times 10^4$ M^{-1}	14.5 μM	6.8 μM
GB5 (**1e**)	$2.7 \pm 0.6 \times 10^4$ M^{-1}	14.7 μM	15.0 μM
GB6 (**1g**)	$4.8 \pm 0.5 \times 10^4$ M^{-1}	51.0 μM	~100 μM
GB7 (**1f**)	$< 1 \times 10^4$ M^{-1}	>100 μM	>100 μM

Table 5
Docking results for the poses obtained with lowest MM-GBSA ΔG_{bind} for each gatorbulin.

Compound	MM-GBSA ΔG_{Bind} (kcal/mol)	RMSD to GB1 Crystal (Å)
GB1 (**1a**)	−72.11	0.51
GB2 (**1b**)	−65.19	0.55
GB3 (**1c**)	−64.64	0.52
GB4 (**1d**)	−72.33	0.51
GB5 (**1e**)	−70.76	0.50
GB6 (**1f**)	−76.84	0.53

2.4. Evaluation of metabolic and physiochemical properties of GB1 and six analogues

Evaluation of metabolic and physiochemical properties of GB1 and six analogues were performed (Table 7). GB1 is highly soluble in pH 7.4 phosphate buffered saline with kinetic solubility greater than 100 μM. All analogues showed similarly high levels of solubility that otherwise, were much higher than that for paclitaxel (a clinically used tubulin-binding compound with kinetic solubility of 1 μM). Hepatic microsome stability was similar for GB1 and all analogues with minimal compound depletion over the course of the incubation. None of the compounds inhibited a panel of human cytochrome P450s. All of the selective controls inhibited more than 80 % and demonstrated selectivity by only inhibiting the correct P450 (Table 7). GB1 and all analogues were minimally bound to plasma proteins with high free fractions. Minor instability was noted in mouse plasma. For most compounds, the percent compound decrease after six hours was less than thirty percent (data not shown). GB4 levels decreased more than other compounds with almost 90 % of the original compound unaccounted for after the six-hour dialysis experiment, potentially due to rapid methyl ester hydrolysis. This may explain the observation that drug levels in the buffer compartment exceeded the plasma compartment for GB4 resulting in a calculated free fraction of 166 %. GB1-6 were predicted to have high passive permeability using PAMPA, where permeability is measured across an artificial membrane. GB7 showed lower permeability than would be anticipated given the results from the other six compounds. GB1 was further evaluated using a cellular model with MDCK cells stably transduced with the human efflux transporter MDR1/P-gp. GB1 showed similar permeability as determined in the PAMPA assay. GB1 also showed equivalent permeability with and against the transporter gradient indicating that GB1 is not a P-gp substrate or is a poor P-gp substrate. Standard pharmacological agents unrelated to tubulin, nadolol served as a negative control and quinidine served as the P-gp positive control. Quinidine had an efflux ratio of 7.1, which was abolished with the addition of the P-gp inhibitor cyclosporin A, demonstrating the assay could identify P-gp substrates.

GB1 was less effective in the engineered SK-OV-3-MDR1-M6/6 cell

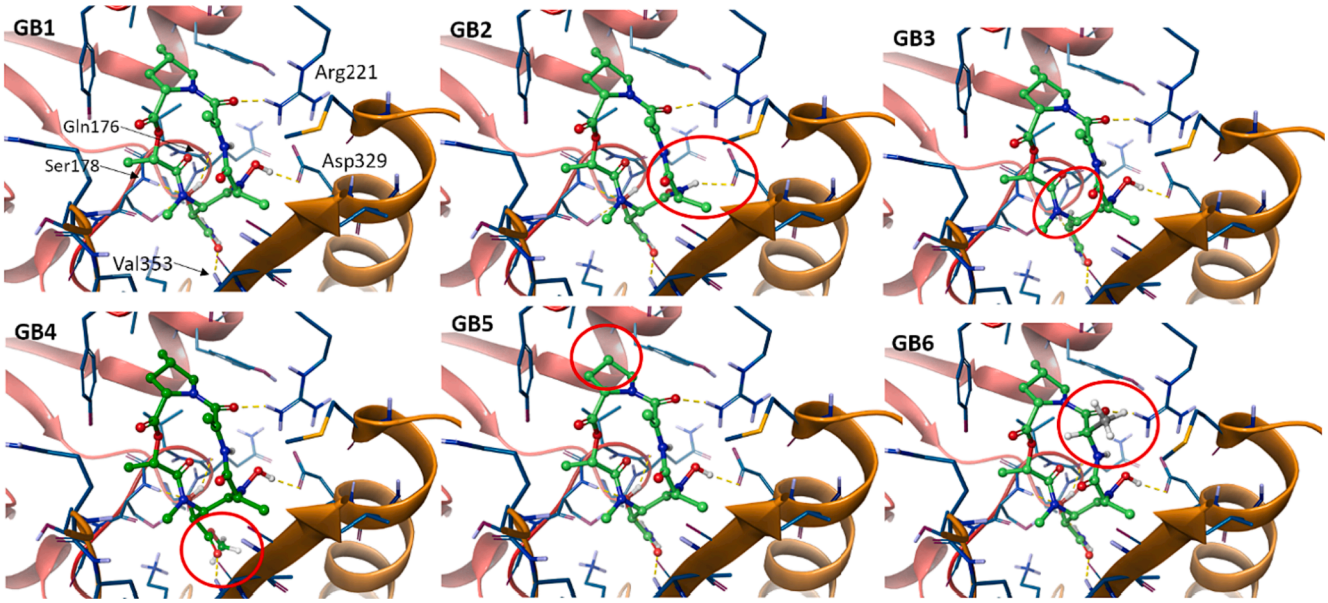

Fig. 6. Docking poses for GB1-6 (**1a-1f**).

Table 6
RMSD between of the representative structure of the clusters and the GB1 structure in the crystal (Å).

Cluster	GB1 (1a)	GB2 (1b)	GB3 (1c)	GB4 (1d)	GB5 (1e)	GB6 (1f)	GB7 (1g)
c0:c1	99:1	92:8	97:3	97:3	96:4	88:12	97:3
0	0.48	0.51	0.47	0.30	0.48	1.43	2.19
1	2.05	2.06	1.86	1.97	2.05	1.51	1.17

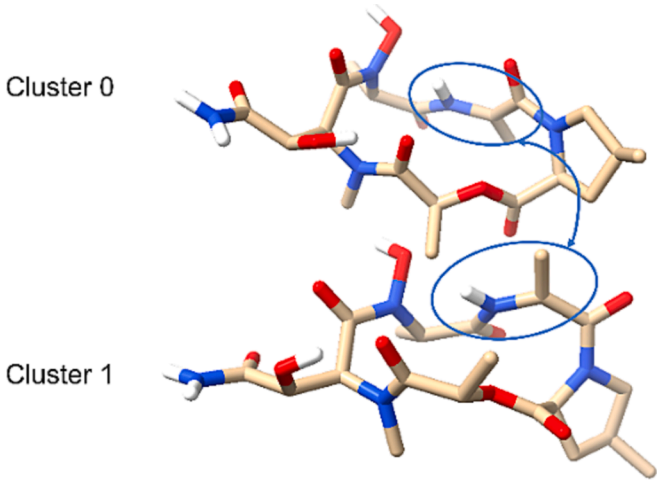

Fig. 7. Representative structures for the two clusters obtained from the simulated annealing calculations for GB1.

line[6] which was credited to P-gp mediated efflux[24]. This is likely caused by the massive overexpression of P-gp, where levels were reported to be 1000x higher than in the parental cell line. With such high transporter expression, even poor substrates may be excluded. Overall, in the context of previous findings, the data suggest that GB1 is a poor P-gp substrate.

3. Conclusion

Building on the robust synthetic route we had established previously, we completed the total synthesis of six simplified analogues of GB1 (**1a**), representing the first-generation analogues. Biological assessment revealed that each amino acid modification that we probed contributed to the biochemical and cellular activity. Furthermore, cevipabulin binds in the same region as gatorbulins, although preferentially targeting α-tubulin compared with GB1 that roughly equally interacts with α- and β-tubulin. Both compounds are structurally and biochemically distinct, as gatorbulins inhibit tubulin polymerization and cevipabulin binds preferentially to the vinca site. Our study demonstrates that tubulin degradation may be achieved by targeting the gatorbulin site. Furthermore, GB1 possesses excellent *in vitro* metabolic and physicochemical properties. GB1 represents a new pharmacological tool to probe biochemical and molecular consequences of engaging the gatorbulin site and may provide novel therapeutic opportunities.

4. Experimental section

4.1. Chemistry

Synthetic chemistry procedures are detailed in the Supporting Information.

4.2. Biology

Protein and ligands. Calf brain tubulin was purified as described[25], and lyophilized for storage. MTC[26]was a kind gift from Prof. Wei-Shuo Fang (Institute of Materia Medica, Beijing). The compounds were diluted in 99.8 % DMSO-d_6 (Merck, Darmstadt, Germany) to a final concentration of 10 mM and stored at − 80 °C.

Polymerization assays. Lyophilized tubulin was suspended in GAB buffer (10 mM NaPi, 30 % glycerol, 1 mM EGTA, 0.1 mM GTP, pH 6.7) in the cold for 20 min. Then, the sample was centrifuged in Optima XPMax Ultracentrifuge at 50 000 rpm, 4 °C and 10 min to remove aggregates. Tubulin concentration was spectrometrically measured and the protein was supplemented with 6 mM $MgCl_2$ and 1 mM GTP. Subsequently, the 96 well plates were prepared by adding 100 μL of GAB buffer containing 25 μM tubulin followed by adding the compounds (podophyllotoxin, GB1-7) at 27.5 μM. Control including 0.5 % DMSO (vehicle) was also included. The absorbance at a wavelength of 350 nm was measured in a Multiskan plate reader.

Measuring of the binding constants. The apparent binding

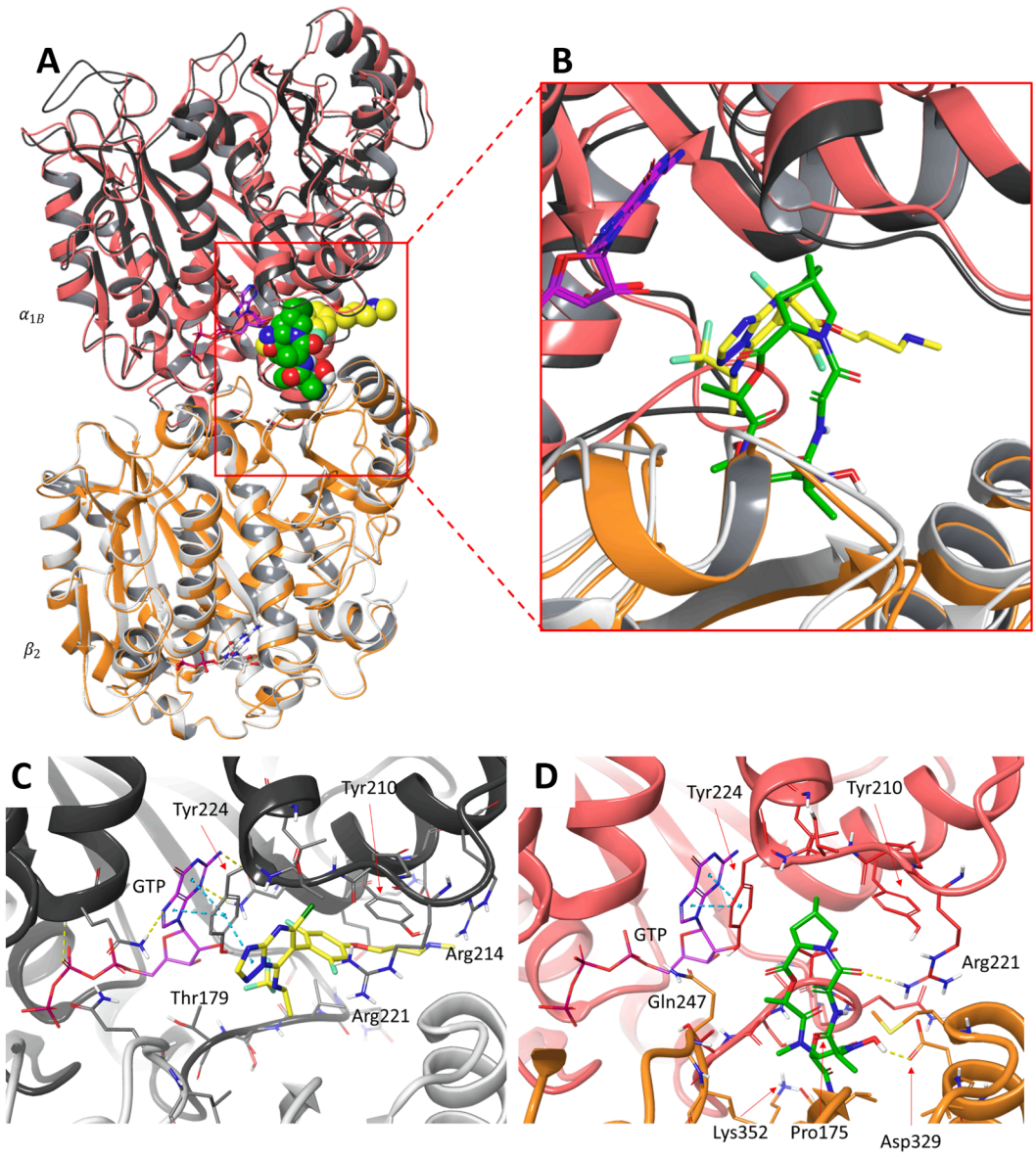

Fig. 8. Comparison of crystal structures of tubulin complexed with cevipabulin (PDBID 7DP8),[9] and GB1 (PDBID:7ALR).[6] In 7DP8 the β 2 chain is in light grey, α 2 in dark grey and cevipabulin in depicted in yellow carbons. In 7ALR the β 2is orange, α 2 in red and GB1 with green carbons. In both cases, GTP is depicted with purple carbons.

constants of GB1 to 7 for the gatorbulin site of tubulin were measured by competition with 2-methoxy-5-(2,3,4-trimethoxyphenyl)-2,4,6-cycloheptatrien-1-one (MTC)[26] as described previously.[6] Briefly, a solution of 10 μM tubulin plus 10 μM MTC was incubated for 30 min with increasing amounts of the compound to be analyzed up to 100 μM. The data from triplicate experiments were analyzed with Equigra V5 as described[27].

Cell culture and MTT viability assay. SK-OV-3 (HTB-77) provided by April Risinger (University of Texas Health Science Center, San Antonio) and HeLa (CCL-2) were from American Type Culture Collection (ATCC; Manassas, VA). SK-OV-3 and HeLa cells were cultured in Earle's modified Eagle's Minimum Essential Medium (EMEM) and Dulbecco's modified Eagle medium (DMEM) respectively, supplemented with 10 % Fetal Bovine Serum (FBS, Sigma, USA) and maintained in 5 % CO_2 at 37 °C in a humidified incubator.

Cells were seeded at 5000 cells/well in 96-well plates, allowed to attach overnight and then treated with different concentrations of GB1–GB7 (**1a–1g**) or solvent control (0.5 % DMSO). Cell viability was measured 48 h following treatment with MTT dye using manufacturer's protocol (Promega). IC_{50} was determined by non-linear regression analysis using GraphPad Prism 8. Data are represented as average ± SD (n = 3).

Immunoblot analysis for tubulin expression in SK-OV-3 cells. Cells were seeded (2×10^5 cells/well) in 6-well clear bottom plates and allowed to attach over 24 h. Media was replaced next day prior to treatment with GB1 (**1a**) or solvent control (0.5 % DMSO) +/- pre-incubation with 10 μM MG-132 (Calbiochem, EMD Millipore Sigma) for 1 h. Whole cell lysates were collected using PhosphoSafe buffer (EMD Chemicals, Inc, Gibbstown, NJ) after 16 h incubation with GB1 (1a). Protein concentrations were measured with the BCA Protein Assay kit (Thermo Fisher Scientific, Rockford, IL). Lysates containing equal amounts of protein were separated by SDS polyacrylamide gel electrophoresis (4–12 %), transferred to polyvinylidene difluoride (PVDF) membranes, probed with primary and secondary antibodies, and detected with the SuperSignal West Femto Maximum Sensitivity Substrate (Thermo Fisher Scientific). Anti-α-tubulin (#2144S), β-tubulin (#2146S), GAPDH (#5174 T) and secondary anti-rabbit (#7074S) antibodies were obtained from Cell Signaling Technology, Inc (Danvers,

Table 7
Metabolic and physicochemical properties of gatorbulins GB1-7 (**1a-1g**).

	Solubility	Liv Mics-$t_{1/2}$		Human P450 Inhibition at 10 μM				Plasma Protein Binding		Permeability-PAMPA		Permeability-MDCK-PgP			
Cpd	Kinetic (μM)	Human min	Mouse min	1A2 %Inh.	2C9 %Inh.	2D6 %Inh.	3A4 %Inh.	Human (%free)	Mouse (%free)	Tested 10^{-6} cm/s	Predicted level	Mean Papp (10^{-6} cm/s) A to B	B to A	Efflux Ratio	Substrate?
GB1	> 100	> 120	> 120	13	< 10	11	< 10	76	80	4.5	high	1.8	1.6	0.9	poor or non-
GB2	> 100	> 120	> 120	< 10	18	< 10	< 10	60	88	8.2	high				
GB3	> 100	> 120	> 120	< 10	< 10	< 10	< 10	69	98	6.2	high				
GB4	> 100	> 120	60.4	< 10	11	< 10	< 10	45	166	9.7	high				
GB5	> 100	> 120	> 120	< 10	< 10	10	< 10	58	85	33.0	high				
GB6	> 100	> 120	> 120	< 10	< 10	< 10	< 10	39	76	4.0	high				
GB7	> 100	> 120	> 120	< 10	< 10	< 10	< 10	72	72	0.7	low				
Pac	1.3														
Sun		34.5	13.5												
Fur				82	< 10	< 10	< 10								
Sul				< 10	94	< 10	21								
Qui				< 10	< 10	88	< 10					1.6	11.1	7.1	yes
Ket				13	39	< 10	98								
Rit								0.5	0.2						
Car								25	36						
Pro										5.7	high				
Ran										0.2	low				
QuC												9.9	9.0	0.9	inhibited (+) ctr
Nad												1.9	1.5	0.8	poor or non-

Note: Pac, paclitaxel; Sun, sunitinib; Fur, furafylline (40 μM); Sul, sulfaphenazole (10 μM); Qui, quinidine (10 μM); Ket, ketoconazole (1 μM); Rit, ritonavir; Car, carbamazepine; Pro, propranolol; Ran, ranitidine; QiC, quinidine + CsA (cyclosporin A); Nad, nadolol.

MA). Densitometry analysis for tubulin quantification was carried out on a representative western blot using ImageJ software and normalized to both GAPDH loading control and solvent control without MG132 pre-incubation (-DMSO).

4.3. Computational modeling

Docking. The molecules were prepared in Schrödinger's Maestro.[28] The receptor was prepared using Maestro's Protein Preparation Wizard, from the crystal structure of the TD1-GB1 complex obtained at 1.93 Å resolution (PDBID:7ALR, Fig. 1)[6] Due to its proximity to the GB1 binding site, GTP was kept in the structure. All other ligands and solvent molecules were removed. The grid box was centered at the GB1 molecule and prepared for peptide docking. The dockings were done with Glide Peptide Docking protocol[29], reserving the 10 poses with lowest GlideSP Binding Energy for each molecule. Finally, each pose was submitted to MM-GBSA optimization of the binding site, including side chains within 3 Å of any ligand atoms, and the final pose with lowest MM-GBSA Binding Energy chosen for the analysis.

Molecular dynamics. The ligands in solution were submitted to simulated annealing molecular dynamics (SAMD) in implicit DMF solvent. The parameters for the ligands were created with Antechamber using GAFF2 and AM1-BCC charges. All molecules were subjected to the same protocol, where first the molecules were simulated for 1 ns at 298 K. For each molecule, 100 structures were sampled at regular intervals from the trajectory obtained, as starting points for the SAMD. Each of the initial structures was submitted to 10 ps heating to 600 K, then cooled to 100 K for the next 13 ps, and finally cooled to 0 K for another 2 ps, totaling 25 ps simulation for each structure. The final conformations where then clustered into two clusters with *cpptraj*. All tools used are part of the AmberTools package for biomolecules simulation[30].

4.4. Measurements of metabolic and physiochemical properties

Solubility. Kinetic solubility was tested from a 10 mM DMSO stock solution by spiking into pre-warmed pH 7.4 phosphate buffered saline in a 96-well plate. The final concentration was 100 μM (1 % DMSO). The plate was maintained at ambient temperature for 24 h on an orbital shaker. Samples were centrifuged through a Millipore Multiscreen Solvinter 0.45 μm low binding PTFE hydrophilic filter plate and were analyzed by HPLC with UV detection at wavelength equals 254 nm. Peak area was compared to standards of known concentration.

Hepatic microsomal stability. Microsome stability was evaluated by incubating 1 μM test compound with 1 mg/mL hepatic microsomes in 100 mM KPi, pH 7.4. The reaction was initiated by adding NADPH (1 mM final concentration). Aliquots were removed at 0, 5, 10, 20, 40, and 60 min and added to acetonitrile (5X, v:v) to stop the reaction and precipitate the protein. NADPH dependence of the reaction was evaluated by setting up incubations without NADPH. At the end of the assay, the samples were centrifuged through a Millipore Multiscreen Solvinter 0.45 μm low-binding PTFE hydrophilic filter plate and analyzed by LC-MS/MS. Data were log-transformed and represented as half-life.

P450 Inhibition. To understand the potential for common drug-drug interactions, P450 inhibition for four major human isoforms were evaluated in human hepatic microsomes by following the metabolism of specific marker substrates (CYP1A2 phenaceten demethylation to acetaminophen; CYP2C9, tolbutamide hydroxylation to hydroxytolbutamide; CYP2D6, bufuralol hydroxylation to 4′-hydroxybufuralol; and CYP3A4, midazolam hydroxylation to 1′-hydroxymidazolam) in the presence or absence of 10 μM probe compound. The concentration of each marker substrate is approximately its Km. Specific inhibitors for each isoform are included in each run to validate the system.

Plasma Protein binding. Plasma protein binding was determined using equilibrium dialysis. All samples were tested in triplicate using the RED Rapid Equilibrium Dialysis Device (Thermo Scientific). The plasma sample was prepared with an initial drug concentration of 2 μM in mouse or human plasma with 0.2 % DMSO. The remaining plasma not loaded into the dialysis chamber was immediately frozen to evaluate the stability of the compound in plasma. Phosphate buffered saline was added to the receiver chamber. The plate was covered with gas permeable film and allowed to shake at 300 RPM at 37ºC for 6 h in a humidified incubator with 5 % CO2 to maintain pH. After six hours, 25 μL was sampled from the plasma and PBS chambers which were then diluted with either blank PBS or plasma to achieve a 1:1 ratio of plasma: PBS for all samples. Five times v:v acetonitrile was added to precipitate protein. Plasma that was not loaded into the RED device was rapidly thawed, diluted 1:1 with PBS and treated with acetonitrile. Drug concentrations were determined by LC-MS/MS. The fraction bound was calculated as ([plasma] – [PBS]) / [plasma].

PAMPA. The assessment of permeability used a commercial PAMPA (Parallel Artificial Membrane Permeability Assay) plate from BD Biosciences (Cat# 353015). Compounds were prepared as DMSO stocks and added to the bottom donor plate containing phosphate-buffered saline, pH 7.4, at a concentration of 5 μM and 1 % final DMSO. Preliminary experiments using phosphate-buffered saline in the top receiver plate showed high non-specific binding. To minimize non-specific binding, 0.4 % w:v lyophilized bovine albumin dissolved in phosphate-buffered saline was used in the top receiver plate. The plates were allowed to incubate at room temperature with shaking, and after 5 h, aliquots were

taken from the donor and receiver plates and analyzed by LC-MS/MS. Compound permeability was calculated using the equation

$$P_e = -\frac{\ln\left[1-\frac{C_A(t)}{C_{eq}}\right]}{(A*\left(\frac{1}{V_D}+\frac{1}{V_A}\right)*t)}$$

where P_e is expressed in units of cm/s, $C_D(t)$**and**$C_A(t)$ are drug concentration in the donor and acceptor at time t, V_D is donor well volume, V_A is acceptor well volume, A is the area of the filter (0.3 cm^2), t is time in seconds, and $C_{eq} = [C_D(t)*V_D + C_A(t)*V_A]/(V_D + V_A)$.

MDCK-MDR1. The MDR1-MDCK cells were provided by Dr Michael Gottesman at the United States National Institutes of Health. **Cell Culture.** Cells were cultured in Dulbecco's Modified Eagle Medium (DMEM) (Gibco, #11995–065) supplemented with 10 % FBS (Gibco, #10082–147), 50 U/ml Penicillin-Streptomycin (Gibco, #15070–063), and 80 ng/ml colchicine (Sigma-Aldrich, #C9754) in a humidified atmosphere of 5 % CO_2 at 37 °C. **Permeability Assay.** Cells were seeded on Greiner Bio-One ThinCert™ inserts at a density of 50,000 cells/well. Testing was usually 4–7 days after plating when the TEER value was greater than 250 Ohms/cm^2. Prior to initiating the assay, the cells were equilibrated in Hank's Balanced Salt Solution (HBSS) with 10 mM HEPES (Stemcell Technologies, #37150) and 0.02 % BSA, pH 7.4 for 1 h at 37 °C with 5 % CO_2 and 95 % relative humidity. Test compound solutions for the donor chambers were prepared at 2 μM in the above buffer, containing 100 μM Lucifer Yellow (LY) (Sigma-Aldrich, #L0144) as the monolayer-integrity marker. The final DMSO concentration was 0.5 % for each test compound. To reduce non-specific binding, the HBSS buffer with 10 mM HEPES was supplemented with 0.5 % BSA in the receiver compartments. The permeability was examined in apical to basolateral (A-B) and basolateral to apical (B-A) directions. Samples were taken at the beginning of the incubation from the donor side, and after 90 min from the donor and receiver compartments and the concentration of drug was determined by LC-MS. LY fluorescence was measured at 430/535 nm using a BioTek Synergy Neo2 microplate reader (Agilent, Santa Clara, CA). LY transport of < 5 % was considered acceptable. Nadolol was used as the negative control and quinidine as positive control for MDR1.

Apparent permeability, P_{app}, was calculated using the equation:

$$P_{app} = \frac{dQ}{dt} \times \frac{1}{A \times C_0}$$

where dQ/dt is the permeability rate, C_0 is the initial concentration in the donor compartment, and A is the surface area of the insert (0.33 cm^2). The ratio of the calculated P_{app} values were used as an efflux ratio.

$$ER = \frac{P_{app}BA}{P_{app}AB}$$

Declaration of Competing Interest

The authors declare the following financial interests/personal relationships which may be considered as potential competing interests: The University of Florida has filed a patent application relating to the content of this article.

Data availability

Data will be made available on request.

Acknowledgments

This work was supported by the National Institutes of Health, NCI grant R01CA172310 (H.L.), the Debbie and Sylvia DeSantis Chair professorship (H.L.) and Ministerio de Ciencia e Innovación PID2021-123399OB-I00 (M.A.O.) PID2019-104545RB-I00 (J.F.D.). We thank Ganadería Fernando Díaz for calf brains supply.

Appendix A. Supplementary material

Synthetic chemistry procedures, retrosynthetic analysis (Figure S1), NMR spectra (Figures S2–S96), computational modeling figures (Figures S97–99), representative original Western blots (Figure S100). This material is available free of charge via the internet at https://www.sciencedirect.com/journal/bioorganic-and-medicinal-chemistry. Supplementary data to this article can be found online at https://doi.org/10.1016/j.bmc.2023.117506.

References

1 Brouhard GJ, Rice LM. Microtubule Dynamics: An Interplay of Biochemistry and Mechanics. *Nat Rev Mol Cell Biol*. 2018;19:451–463. https://doi.org/10.1038/S41580-018-0009-Y.
2 Desai A, Mitchison TJ. Microtubule Polymerization Dynamics. *Annu. Re. Cell Dev. Biol.* 1997;13:83–117. https://doi.org/10.1146/annurev.cellbio.13.1.83.
3 Dalbeth N, Lauterio TJ, Wolfe HR. Mechanism of Action of Colchicine in the Treatment of Gout. *Clin Ther*. 2014;36:1465–1479. https://doi.org/10.1016/J.CLINTHERA.2014.07.017.
4 Kaul R, Risinger AL, Mooberry SL. Microtubule-Targeting Drugs: More than Antimitotics. *J. Nat. Prod.* **2019**, *82* (3), 680–685. https://doi/10.1021/acs.jnatprod.9b00105.
5 Risinger AL, Du L. Targeting and Extending the Eukaryotic Druggable Genome with Natural Products: Cytoskeletal Targets of Natural Products. *Nat Prod Rep*. 2020;37:634–652. https://doi.org/10.1039/C9NP00053D.
6 Matthew S, Chen QY, Ratnayake R, Fermaintt CS, Lucena-Agell D, Bonato F, Pet al. Gatorbulin-1, a Distinct Cyclodepsipeptide Chemotype, Targets a Seventh Tubulin Pharmacological Site. *Proc. Natl. Acad. Sci. U. S. A.* **2021**, *118* (9) e2021847118. https://doi.org/10.1073/PNAS.2021847118.
7 Singh SB. Discovery and Development of Dolastatin 10-Derived Antibody Drug Conjugate Anticancer Drugs. *J Nat Prod*. 2022;85:666–687. https://doi.org/10.1021/ACS.JNATPROD.1C01135.
8 Reader JC, Fan C, Ory ECH, et al. Microtentacle Formation in Ovarian Carcinoma. *Cancers*. 2022;14:800. https://doi.org/10.3390/CANCERS14030800.
9 Yang J, Yu Y, Li Y, et al. Complex Reveals a Novel Agent Binding Site on α-Tubulin with Tubulin Degradation Effect. *Sci Adv*. 2021;7:eabg4168. https://doi.org/10.1126/SCIADV.ABG4168.
10 Kim B, Park H, Salvador LA, et al. Evaluation of Class I HDAC Isoform Selectivity of Largazole Analogues. *Bioorg Med. Chem. Lett.* 2014;24:3728–3731. https://doi.org/10.1016/J.BMCL.2014.07.006.
11 Chen QY, Liu Y, Cai W, Luesch H. Improved Total Synthesis and Biological Evaluation of Potent Apratoxin S4 Based Anticancer Agents with Differential Stability and Further Enhanced Activity. *J Med Chem*. 2014;57:3011–3029. https://doi.org/10.1021/JM4019965.
12 Doi T, Numajiri Y, Munakata A, Takahashi T. Total Synthesis of Apratoxin A. *Org Lett*. 2006;8:531–534. https://doi.org/10.1021/OL052907D.
13 Li P, Xu JC. 1-Ethyl 2-Halopyridinium Salts, Highly Efficient Coupling Reagents for Hindered Peptide Synthesis Both in Solution and the Solid-Phase. *Tetrahedron*. 2000;56:8119–8131. https://doi.org/10.1016/S0040-4020(00)00657-8.
14 Takano S, Moriya M, Ogasawara K. A Concise Stereocontrolled Total Synthesis of (+)-Estrone. *Tetrahedron Lett*. 1992;33:1909–1910. https://doi.org/10.1016/S0040-4039(00)74175-X.
15 Aurelio L, Brownlee RTC, Hughes AB. A Novel Synthesis of N-Methyl Asparagine, Arginine, Histidine, and Tryptophan. *Org Lett*. 2002;4:3767–3769. https://doi.org/10.1021/OL026799W.
16 Hale KJ, Manaviazar S, George JH, Walters MA, Dalby SM. Total Synthesis of (+)-Azinothricin and (+)-Kettapeptin. *Org Lett*. 2009;11:733–736. https://doi.org/10.1021/OL802817T.
17 Hale KJ, Manaviazar S, George JH. Total Synthesis of (+)-A83586C, (+)-Kettapeptin and (+)-Azinothricin: Powerful New Inhibitors of β-Catenin/TCF4- and E2F-Mediated Genetranscription. *Chem Commun*. 2010;46:4021–4042.
18 Nicolaou KC, Estrada AA, Zak M, Lee SH, Safina BS. A Mild and Selective Method for the Hydrolysis of Esters with Trimethyltin Hydroxide. *Angew. Chemie - Int. Ed.* 2005;44:1378–1382. https://doi.org/10.1002/ANIE.200462207.
19 Ley SV, Prieur A, Heusser C. Total Synthesis of the Cyclic Heptapeptide Argyrin B: A New Potent Inhibitor of T-Cell Independent Antibody Formation. *Org Lett*. 2002;4:711–714. https://doi.org/10.1021/OL017184M.
20 Kogen H, Kiho T, Nakayama M, Furukawa Y, Kinoshita T, Inukai M. Crystal Structure and Total Synthesis of Globomycin: Establishment of Relative and Absolute Configurations. *J Am Chem Soc*. 2000;122:10214–10215. https://doi.org/10.1021/JA002547J/SUPPL_FILE/JA002547J_S.PDF.
21 Agarkov A, Greenfield SJ, Ohishi T, Collibee SE, Gilbertson SR. Catalysis with Phosphine-Containing Amino Acids in Various "Turn" Motifs. *J Org Chem*. 2004;69:8077–8085. https://doi.org/10.1021/JO049103G.
22 Kovalevich J, Cornec AS, Yao Y, et al. Characterization of Brain-Penetrant Pyrimidine-Containing Molecules with Differential Microtubule-Stabilizing Activities Developed as Potential Therapeutic Agents for Alzheimer's Disease and Related

Tauopathies. *J Pharmacol Exp Ther*. 2016;357:432–450. https://doi.org/10.1124/JPET.115.231175.
23 Beyer CF, Zhang N, Hernandez R, et al. TTI-237: A Novel Microtubule-Active Compound with in Vivo Antitumor Activity. *Cancer Res*. 2008;68:2292–2300. https://doi.org/10.1158/0008-5472.CAN-07-1420.
24 Du L, Yee SS, Ramachandran K, Risinger AL. Elucidating Target Specificity of the Taccalonolide Covalent Microtubule Stabilizers Employing a Combinatorial Chemical Approach. *Nat Commun*. 2020;11:654. https://doi.org/10.1038/s41467-019-14277-w.
25 Andreu JM. in *Methods Mol. Biol.* Vol. 137 (ed J. Zhou) Ch. Microtubule Protocols, 17– 28 (Humana Press Inc., 2007).
26 Fitzgerald TJ. Molecular Features of Colchicine Associated with Antimitotic Activity and Inhibition of Tubulin Polymerization. *Biochem Pharmacol*. 1976;25:1383–1387. https://doi.org/10.1016/0006-2952(76)90108-8.
27 Diaz JF, Buey RM. Characterizing Ligand-Microtubule Binding by Competition Methods. *Methods Mol. Med*. Vol. 137 (ed J. Zhou), 245–260 (Humana Press Inc., 2007).
28 Schrödinger LLC. Maestro, Version 12.1.013; Schrödinger, LLC: New York, NY, USA, NY, USA, **2019**.
29 Tubert-Brohman I, Sherman W, Repasky M, Beuming T. Improved Docking of Polypeptides with Glide. *J Chem Inf Model*. 2013;53:1689–1699. https://doi.org/10.1021/CI400128M.
30 Case DA, Belfon K, Ben-Shalom IY, Brozell SR, Cerutti DS, Cheatham TEet al.. AMBER 20. University of California: San Francisco **2020**.